Relationship between spatial scale of pathogen dispersal and host landscape that minimizes infection rate in agricultural crops

Yevhen F. Suprunenko[1,*] and Christopher A. Gilligan[1,‡]

Department of Plant Sciences, University of Cambridge, Downing Street, Cambridge, CB2 3EA, UK
*,‡Corresponding authors: * ys526@cam.ac.uk; ‡ cag1@cam.ac.uk
Yevhen F Suprunenko (0000-0001-5927-7571) - ORCID
Christopher Gilligan (0000-0002-6845-0003) - ORCID

Abstract

The initial rate of invasion of crop pathogens depends on the degree of spatial aggregation of susceptible crops and the dispersal characteristics of the pathogen. We introduce an analytical approach to identify the largest degree of aggregation that minimises the initial infection rate of an invading pest or pathogen. The degree of aggregation is described in terms of the size of clusters of crop fields within a landscape and the corresponding separation distance between these clusters. Results are calculated for several common dispersal kernels including the Gaussian, negative exponential, and power-law kernels, and can be extended to other dispersal kernels. Our analytical results align well with computer simulations of an individual-based model for pathogen invasion and spread through a broad range of artificial host landscapes. We also analysed an example of the dispersal of cassava brown streak virus through a realistic cassava landscape. The results of this paper can assist crop growers, advisers and regulators by providing insights into spatial configurations of host landscapes that most effectively slow the spread of invading pathogens.

1. Introduction

One of the key factors that determine how fast a crop pathogen invades and spreads across an agricultural landscape is the relationship between the dispersal scale of the pathogen and the spatial distribution of susceptible crops in the landscape (1–12). It is possible to slow the rate of pathogen invasion by adjusting the spatial scale of host distribution relative to the intrinsic scale of pathogen dispersal (7–12), for example by reducing host aggregation (13–16), growing resistant varieties (17) or application of fungicide. Two simple measures of pathogen invasion are the rate, r, at which susceptible fields become infected at the start of an epidemic, and the closely related quantity R_0, the basic reproduction number as $R_0 = r/\mu$ where $1/\mu$ is the average infectious period of infected hosts. Insights from theoretical (7–10) and experimental (11,12) studies indicate that invasion is slowed and r and R_0 decline as the host landscape becomes more dispersed. While this could imply that the minimal values of r and R_0 would occur when fields were evenly dispersed, recent theoretical work (18) has shown that r and R_0 can be minimized in agricultural landscapes with many different spatial

configurations in which fields with susceptible crops can be aggregated into clusters up to a threshold size. Suprunenko *et al.* (18) illustrated the process for artificial landscapes with a fixed area of susceptible crops distributed spatially in clusters of different sizes on a regular square lattice (18), figure 1a. Given the total area of crop was fixed, the number, $N_{clusters}$, of clusters decreased as cluster size increased. The largest degree of aggregation (i.e. the smallest $N_{clusters}$) associated with minimum *r* can be characterised by a threshold cluster size of width, L_H^*, and separation distance between clusters, Δ_H^* (cf figure 1c). The threshold values, L_H^* and Δ_H^*, are expected to be functions of the pathogen dispersal kernel, $b(x)$. Therefore, the association between L_H^*, Δ_H^* and $b(x)$ constitutes the relationship between spatial scales in epidemics that minimizes the infection rate. Knowledge of the threshold values, L_H^* and Δ_H^* would be a valuable tool for agricultural planners to understand and to minimise the risk of invasion of a pathogen (or pest) for which the dispersal characteristics are known.

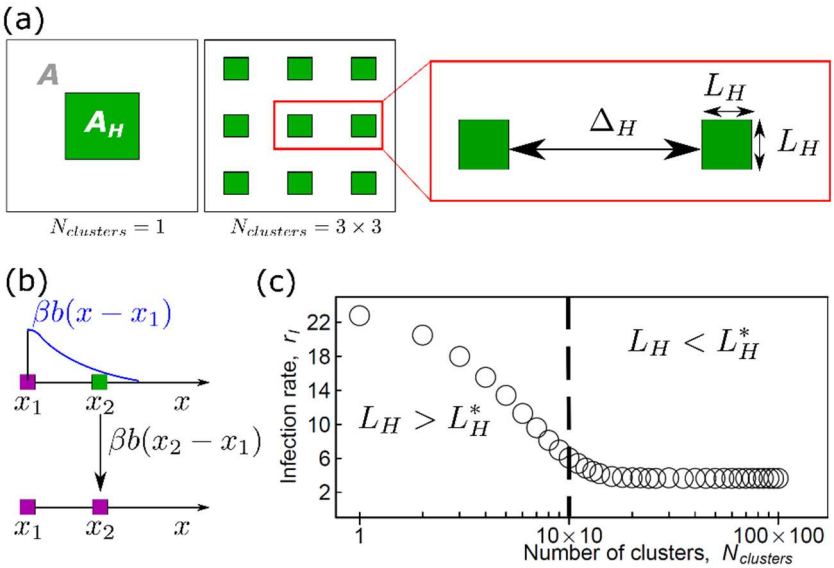

Figure 1. The infection rate of susceptible agricultural crop fields becoming infected at the start of an epidemic can be minimized by a range of different spatial re-configurations of a landscape. (a) An illustration of a crop area, A_H, green, that is aggregated in one cluster, $N_{clusters} = 1$, or nine clusters, $N_{clusters} = 3 \times 3$, placed on a regular square grid within an agricultural landscape, A, where arbitrarily $A_H A^{-1} = 0.15$. The degree of aggregation (clustering) is characterised by the number of clusters, $N_{clusters}$, that determine the size, L_H, of a square cluster and separation distance, Δ_H between clusters. **(b)** A single infected field (magenta square) is a source of infection for a susceptible field (green square) according to a dispersal rate per contact density, β, and a dispersal kernel $b(x)$. **(c)** The reconfiguration of crop area A_H into clusters of size L_H that are smaller than a threshold size L_H^*, $L_H < L_H^*$, decreases the infection rate from its maximal value (that corresponds to $N_{clusters} = 1$) to its minimal value (that corresponds with $N_{clusters} \geq N_{clusters}^*$, where $N_{clusters}^*$ is the threshold number of clusters). The illustration is a modified version of figure 1

in Suprunenko *et al.* (18). Computer codes for all figures in the current paper are available from Figshare, see (19).

Computer simulation of epidemic models on simulated landscapes can, in principle, be used to derive estimates for the threshold size L_H^* and separation distance Δ_H^* for a given pathogen dispersal (20,21). The solution is obtained by considering epidemics on host landscapes with many different spatial configurations and identifying the range of degrees of aggregations of hosts that corresponds to minimising r. However, realistic epidemic spread models may be difficult to construct for each new pest or pathogen and, moreover, the need to consider a large number of different spatial configurations is computationally demanding and, arguably, inefficient.

Here, we explore an alternative approach to identify landscapes that minimise initial infection rates using an analytical approximation for the initial rate of infection, r. We test the analytical approximation for infection rates against empirical infection rates derived from computer simulations of an individual-based model (IBM) for pathogen invasion and spread through a host landscape. Using the analytical approximation for r, we derive values for L_H^* and Δ_H^* for a range of generic host landscapes and commonly-used dispersal kernels that include the Gaussian, negative exponential, power-law kernels and others. We illustrate a potential application of the approach motivated by the spread of cassava brown streak virus (CBSV) that threatens cassava production in sub-Saharan Africa (22–24). Using a dispersal kernel for CBSV estimated by Godding *et al.* (25), and a section of a cassava landscape provided by Szyniszewska (26), we provide examples of maps showing estimates of local threshold sizes (and separation distances) of clusters of cassava fields that minimise infection rate.

2. Methods

2.1 Mathematical approximation for infection rate

We consider a susceptible-infected (SI) epidemiological compartmental individual-based model (IBM) for the invasion and spread of a pathogen through an agricultural landscape partially occupied by susceptible host crops. An expression for the infection rate, r, has been variously derived in a number of studies including Bolker (7), North and Godfray (10), van den Bosch *et al.* (27) and others (9,18,28,29). For example, consider the approximation from (18):

$$r = \beta \times \left(n_S + \frac{n_S}{n^2} \int_0^{\frac{\sqrt{A}}{2}} 2\pi x b(x) g(x) \mathrm{d}x \right), \qquad (2.1)$$

where β is the infection rate per contact density and $b(x)$ is the pathogen dispersal kernel as a function of distance x; the host landscape is assumed to be a square plot of land with area A partially occupied by land containing a target crop consisting of N sufficiently small identical, individual fields with area A_0; each field is treated as an individual 'host' described

as a point-like object located at the centre of a field; the initial densities $n_S = (N-1)A^{-1}$ and $n = NA^{-1}$ are the densities of susceptible and all, N, hosts respectively; the total area occupied by hosts is A_H, i.e. $A_H = A_0 N$, where $A_H \leq A$; $g(x)$ denotes the second order spatial cumulant (also known as a truncated correlation function or autocovariance, e.g. see (30,31)) that characterises the spatial structure of a host landscape.

The expression inside the brackets in equation (2.1) represents the spatial density of contacts with susceptible crops (i.e. fields) from a randomly located initial infected field. Similarly, van den Bosch *et al.* (27) recently described an equivalent product $b(x)g(x)$ (cf equation 2.1) as one that "describes how a pathogen 'sees' the host population around an infected host individual". Based on these insights, we construct an explicit expression for the spatial density of contacts to substitute for the expression in brackets in equation (2.1). We use the following approach: while an IBM ordinarily considers individual hosts as point-like objects, we consider individual hosts explicitly as fields, i.e. as square plots of cropped land with area A_0. We denote the spatial density of fields (measured as the number of fields per area) at location $\boldsymbol{x}$ as $n(\boldsymbol{x})$, and define $n(\boldsymbol{x}) = A_0^{-1}$ when a point $\boldsymbol{x}$ lies within a field, and $n(\boldsymbol{x}) = 0$ when $\boldsymbol{x}$ is outside a field. A pathogen at location $\boldsymbol{x}$ can infect directly the density of fields $n_b(\boldsymbol{x})$, where

$$n_b(\boldsymbol{x}) = \int b(|\boldsymbol{x_0} - \boldsymbol{x}|) n(\boldsymbol{x_0}) \mathrm{d}\boldsymbol{x_0} \,,$$

and the integration is over the entire landscape. Averaging the value $n_b(\boldsymbol{x})$ over all possible locations, $\boldsymbol{x}$**,** within the landscape leads to the quantity $\bar{n}$,

$$\bar{n} \;= (\int n_b(\boldsymbol{x}) n(\boldsymbol{x}) d\boldsymbol{x}) / (\int n(\boldsymbol{y}) \mathrm{d}\boldsymbol{y}),$$

that can be interpreted as the spatially averaged density of contacts (with susceptible crops) that can result in infection from an initial randomly infected crop. Therefore, the expression in brackets in equation (2.1) can be estimated by the density $\bar{n}$, i.e.

$$r = \beta \times \bar{n}. \tag{2.2}$$

Further to this, we make the following two simplifying approximations.

Approximation 1**:** Here, we develop an approximation for equation (2.2) when there is a high degree of aggregation of the target crop within a landscape (i.e. when $N_{clusters}$ is small): $r \approx \beta \times \bar{n}_1(L_H)$, where $\bar{n}_1(L_H)$ is derived as follows. We assume that the crop area is distributed into identical $L_H \times L_H$ square clusters on a regular square lattice, as illustrated in figure 1a. The total number of clusters is $N_{clusters}$. We denote the spatial density of crops within a single cluster as $n_1(\boldsymbol{x})$ where $n_1(\boldsymbol{x}) = A_0^{-1}$ if $0 \leq x_1 \leq L_H$ and $0 \leq x_2 \leq L_H$ and $n_1(\boldsymbol{x}) = 0$ otherwise. Given a high degree of aggregation, i.e. when all hosts are aggregated into a small number of large clusters, we estimate r on a single cluster and use $n_1(\boldsymbol{x})$ instead of $n(\boldsymbol{x})$ in the expression (2.2) and obtain $\bar{n}_1$ instead of $\bar{n}$ where $\bar{n}_1 \;= (\int n_b(\boldsymbol{x}) n_1(\boldsymbol{x}) d\boldsymbol{x}) / (\int n_1(\boldsymbol{y}) \mathrm{d}\boldsymbol{y})$. Using straightforward algebraic transformations, shown in the electronic supplementary material (Supplementary Note 1), the expression for $\bar{n}_1$ is simplified further:

$$\bar{n}_1(L_H) = 4L_H^2 A_0^{-1} \int_0^1 \int_0^1 \mathrm{d}x\mathrm{d}y\, b(L_H\sqrt{x^2+y^2})(1-x)(1-y). \tag{2.3}$$

The quantity $\bar{n}_1$ denotes the averaged density of fields within a single cluster that a randomly introduced infected field within that cluster can infect directly via a dispersal kernel $b(x)$. The upper bound of the quantity $\bar{n}_1$ is A_0^{-1}, i.e. a density of crops within a single cluster.

Approximation 2: Here, we develop an approximation for equation (2.2) when there is a low degree of aggregation of a host landscape, $r \approx \beta \times n$. We assume that the pathogen dispersal kernel, $b(x)$, is sufficiently long-ranged with respect to an individual field of area A_0, i.e. the characteristic dispersal length, a, should be larger than the size of an individual field, $a > \sqrt{A_0}$. Consequently, the minimum value of the infection rate can be approximated as $r_{min} = \beta \times n$, where n is the spatial density of all N fields of a host crop within the landscape with area A, $n = NA^{-1}$. For a low degree of aggregation we therefore use $r \approx r_{min}$.

Finally, by combining expressions for the infection rate within a single cluster, $\beta \times \bar{n}_1(L_H)$, and its minimal value, $\beta \times n$, we use the following approximation for r, denoted as $r^{approximate}$:

$$r^{approximate} = \beta \times \max[\bar{n}_1(L_H), n]. \tag{2.4}$$

It is important to stress that the approximation is applicable to dispersal kernels, $b(x)$, that are decreasing functions with distance x. For dispersal kernels that do not decrease monotonically with distance, e.g. for an inverse Gaussian (Wald) dispersal or lognormal dispersal kernel (see Nathan et al. (32)) the infection rate does not necessarily decrease when the number of clusters ($N_{clusters}$) increases.

2.2 Computer simulations of an individual-based model

To test the approximation we compare the performance of equation (2.4) with empirical rates for *r* at the start of an epidemic from computer simulations of an individual-based model of invasion for pathogen spread in an agricultural landscape (18). For convenience, details of the individual-based model are summarised in Appendix A. We observed good agreement between analytical estimates (equation 2.4) and simulations for different relative values of characteristic spatial scales in an epidemic (figure 2), and, therefore, proceed to use this approximation to find the relationship between spatial scales that minimize the infection rate $r^{approximate}$.

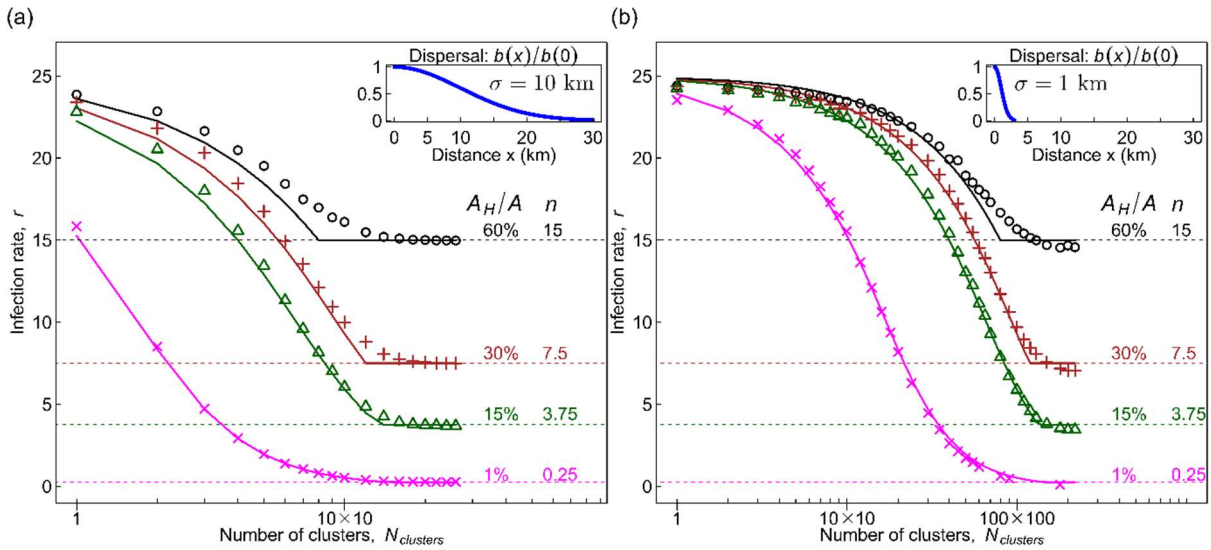

Figure 2. Analytical approximation for infection rate (equation 2.4) compared with estimates inferred from computer simulations of an individual-based model. Results are shown for two different dispersal kernels given by a Gaussian function with standard deviation: **(a)** $\sigma = 10$ km, panel **(b)** $\sigma = 1$ km. The quantity $A_H A^{-1}$ denotes the fraction of the landscape occupied by susceptible fields; $n = NA^{-1}$ is the spatial density of all N crop fields in the landscape with area A. Here, $\beta = 1$, and the area of a unit field is $A_0 = 0.04$ km^2; the upper bound of the rate r is given by, $\beta A_0^{-1} = 25$. The data (33) from computer simulations of individual-based model of invasion and spread of pathogens in agricultural landscapes are taken from Suprunenko *et al.* (18); codes used in the current paper are available online from Figshare (19).

2.3 Mathematical approximation for threshold size and separation distance

We define the threshold size L_H^* as the value of the argument of the function $\bar{n}_1(L_H)$ in equation (2.4) such that

$$\bar{n}_1(L_H^*) = n. \tag{2.5}$$

Using the definition $n = NA^{-1} = A_H(AA_0)^{-1}$, the condition (2.5) can be re-written as

$$\bar{n}_1(L_H^*)A_0 = A_H A^{-1}. \tag{2.6}$$

The right-hand side of equation (2.6) is a dimensionless parameter $A_H A^{-1}$ denoting the fraction of the landscape occupied by susceptible fields. For the most typical dispersal kernels, $b(x)$, that are characterized by a scale parameter, a, (see Appendix B, table B1), the left-hand side of equation (2.6) depends on the dimensionless parameter $L_H^* a^{-1}$ explicitly (see electronic supplementary material, Supplementary Note 2 for details). Therefore, for a landscape characterized by $A_H A^{-1}$, the equation (2.6) determines L_H^* in units of the scale parameter, a, that characterises the pathogen dispersal kernel $b(x)$. The threshold separation distance Δ_H^* is then determined (on a regular square lattice, figure 1a) by L_H^* and $A_H A^{-1}$:

$$\Delta_H^* = L_H^* \times \left(\sqrt{A/A_H} - 1\right). \quad (2.7)$$

Parameters and functions used in the current paper are summarized in Table 1.

Table 1. Parameters used in the model, together with spatial scales of pathogen dispersal and host landscape and their threshold values.

Symbol	Description
	Model parameters
A	Entire area of the landscape, a square plot of land.
A_0	Area occupied by a single field of host crop (a square plot of cropped land).
N	Number of host crop fields within the landscape.
A_H	Total area occupied by fields (host crop), $A_H = A_0 \times N;\ A_H \leq A$.
n	Density of all host crop fields within a landscape, $n = N/A$.
n_S	Density of susceptible fields within a landscape, assuming a single initial infected field, $n_S = (N-1)/A$.
$b(x)$	Pathogen dispersal kernel.
r	Rate of infection of susceptible fields at the start of an epidemic, equation (2.1).
	Spatial scales and degree of aggregation of a host landscape
a, b_0	Scale parameter (a) and a shape parameter (b_0) of a pathogen dispersal kernel, see table B1.
L_H, Δ_H	Cluster size (L_H) and separation distance (Δ_H) characterising a host crop landscape, figure 1a.
$N_{clusters}$	Number of clusters of cropped fields within the landscape, $N_{clusters} = A_H/L_H^2 = A/(L_H + \Delta_H)^2$. It can be seen as a measure of the degree of aggregation of a host landscape.
	Threshold values
L_H^*, Δ_H^* $N_{clusters}^*$	Threshold values of cluster size (L_H^*) and separation distance (Δ_H^*), figure 1c, expressed in units of the scale parameter a and calculated from equations (2.6) and (2.7). $N_{clusters}^*$ is the corresponding threshold value of the number of clusters.

3. Results

3.1 Influence of spatial scales on infection rate

To understand how the relationship between spatial scales of pathogen dispersal and host landscape influences an epidemic, we used the rate r, equation (2.1), at which susceptible hosts (i.e. fields with susceptible crops) become infected at the start of an epidemic. We developed an approximation for the rate r (equation 2.4, figure 2) that allowed us to study the influence of spatial scales. Here, the spatial scale of pathogen dispersal (represented by a dispersal kernel $b(x)$) is characterised by a scale parameter, a, as summarized by Nathan *et al.* (32) for some of the most commonly used dispersal kernels (see Appendix B table B1 for a

summary). To characterize the spatial scales of a host landscape, we consider that: (i) the fraction $A_H A^{-1}$ of the landscape is occupied by susceptible crops, (ii) crops are aggregated spatially in square $L_H \times L_H$ clusters on a regular square lattice (cf figure 1a) where clusters are separated by distance Δ_H. Thus, the spatial scales of a host landscape are characterized by the cluster size, L_H, and by the corresponding separation distance, Δ_H.

Using the approximation for the rate r (equation 2.4, figure 2), we identified a range of values of cluster size, L_H, for which the infection rate r is minimized. Within the identified range, the largest value of the cluster size L_H is referred to as a threshold cluster size L_H^*; equation (2.6) determines the ratio of the threshold cluster size to the pathogen dispersal scale parameter, $L_H^* a^{-1}$, for given $A_H A^{-1}$ and $b(x)$. Correspondingly, the threshold separation distance is calculated from equation (2.7). Thus, the resulting values of $L_H^* a^{-1}$ and $\Delta_H^* a^{-1}$ describe the relationship between spatial scales that minimize the infection rate r in an epidemic of a given pathogen in a host landscape.

3.2 Results for dispersal kernels defined in table B1

To illustrate the application of the approach to different dispersal kernels and landscapes, we first consider the Gaussian, negative exponential, power-law kernels and other kernels (see Appendix B, table B1 for more details). The results are summarised in figure 3 for the exponential and power-law kernels, while the results for the other kernels from table B1 are shown in the electronic supplementary material, Supplementary Note 4. In addition to the numerical solution for L_H^* from equation (2.6), we derived an explicit analytical estimate for L_H^* when the value of $A_H A^{-1}$ is small. In that case, the value of L_H^* is also small; therefore, using an approximation $b\left(L_H^* \sqrt{x^2 + y^2}\right) \approx b(0)$ in equation (2.6) we derived:

$$L_H^* \approx \sqrt{\frac{A_H}{b(0)A}}, \qquad \text{when} \quad \frac{A_H}{A} \ll 1. \tag{3.1}$$

The estimate (3.1), shown by grey curves in figure 3, demonstrates broad agreement with the numerical solution for L_H^* from equation (2.6).

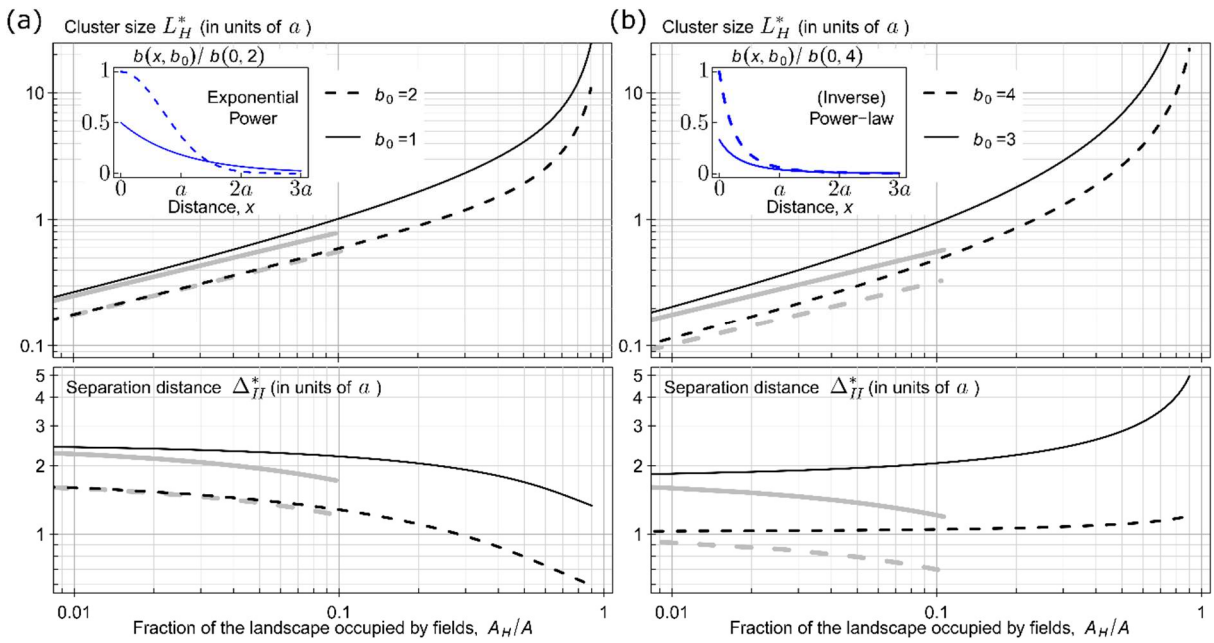

Figure 3. Threshold cluster size L_H^* and threshold separation distance Δ_H^* identified for two types of dispersal kernels. (a) Results are shown for the exponential power kernels that correspond to the Gaussian kernel when $b_0 = 2$, and negative exponential when $b_0 = 1$, shown in the inset of the panel. **(b)** Results are shown for inverse power-law kernels with exponents $b_0 = 3$ and $b_0 = 4$, shown in the inset of the panel. See table B1 in Appendix B for exact analytical expressions for the dispersal kernels used here. In both panels black curves represent numerical estimates from equations (2.6) and (2.7), grey curves at $A_H A^{-1} \leq 0.1$ represent explicit analytical estimates from equations (3.1) and (2.7). The R and Mathematica codes used to calculate these results are available from Figshare (19) and can be easily applied to other dispersal kernels.

We present an example on how results, shown in figure 3, could inform stakeholders including farmers and other agricultural planners on the spatial structure of a host landscape. First, to keep the infection rate at the start of an epidemic at its minimal value $r_{min} = \beta n$, no cluster of hosts in a given landscape should be larger than $L_H^* \times L_H^*$. In addition, each $L_H^* \times L_H^*$ cluster should be surrounded by a host-free zone of width $\Delta_H^*/2$. The same principle applies to clusters of a smaller size $L_H < L_H^*$: any $L_H \times L_H$ clusters should be surrounded by a host-free zone of width $\Delta_H/2$, where $\Delta_H = L_H\left(\sqrt{A/A_H} - 1\right)$, (cf equation (2.7)). The zones around different clusters should not overlap, i.e. if there are two clusters within the landscape, $L_H^{(1)} \times L_H^{(1)}$ and $L_H^{(2)} \times L_H^{(2)}$, where both sizes are below the threshold size, i.e. $L_H^{(1),(2)} \leq L_H^*$, then the minimal suggested separation distance between these clusters equals half the sum of the corresponding separation distances, i.e. $(\Delta_H^{(1)} + \Delta_H^{(2)})/2$.

Although here we considered the spatial distribution of the cropped area into square clusters on a square regular lattice, other geometrical configuration could be considered. For example,

assuming the cropped area is distributed among long narrow fields (e.g. see (12)) we derived the explicit analytical estimate for L_H^* analogous to equation (3.1); see Appendix C.

In addition, the analytical results in figure 3 provide some general insights into the role that the spatial scale parameter, a, and the shape parameter, b_0, (cf Table B1 in Appendix B) of a dispersal kernel play in epidemics. The insights can be used for a quick comparison of how quickly pathogens characterised by different dispersal kernels would invade the same host landscape. From equation (2.6) and its dependence on the dimensionless parameter L_H^*/a it follows that an increase of the spatial scale parameter a (i.e. an increase of dispersal length) reduces the infection rate at the start of an epidemic towards its minimal value βn, see Appendix D for the details. Considering the role of the parameter b_0 it can be observed in Figure 3a that the values of L_H^* for the negative exponential kernel ($b_0 = 1$) are larger than for Gaussian kernel ($b_0 = 2$). This result means that in the same host landscape the infection rate r at the start of an epidemic will be higher for the Gaussian kernel than for the negative exponential kernel (assuming β is constant).

3.3 Results for a dispersal kernel of cassava brown streak virus

For a real-life example, we considered the invasion of CBSV through a cassava landscape. The corresponding epidemic spread model was developed by Godding *et al.* (25). By fitting an epidemiological model with a dispersal kernel to surveillance data, Godding *et al.* (25) derived posterior distributions for parameters of a power-law kernel for CBSV dispersal kernel; the dispersal kernel was defined on a raster with 1 km spatial resolution imposed by the spatial resolution of the available data on host distribution (26). Here, using results from Godding *et al.* (25), we selected the power-law dispersal kernel $b(x)$ characterised by the following two parameters, $\alpha = 3.75$, the exponent, and $p = 0.12$, where *p* defines the kernel value within the source cell; the kernel $b(x)$ is shown as an inset in figure 4a. To illustrate the application of the analytical approach we, in common with Godding *et al.* (25), use CassavaMap (26) as a source of mapped landscape data for cassava. The landscape data for cassava are derived (25) from production statistics (26) and resolved to 1 km^2 raster cells across sub-Saharan countries that cultivate cassava. The analytical estimates (2.6)-(2.7) depend on the ratio of host crop area A_H and the total area A. We express the landscape in terms of hectares of cassava fields per raster cell taking account that, according to Szyniszewska (26), no more than half of the area of each raster cell can be allocated to cassava production (approx. 50 hectares). Therefore, the maximum value of $A_H A^{-1}$ in the data on the cassava landscape cannot be larger than 0.5, i.e. here $A_H A^{-1} \leq 0.5$.

Using the approach described above, we calculated L_H^* and Δ_H^* (figure 4a-b). Note, the step-like structure of the dispersal kernel leads to an exceptionally close agreement between an estimate of L_H^* given by equation (3.1) and the numerical estimate from equation (2.6). We use an area $A = 24 \times 24$ km^2 of a landscape in an arbitrarily selected region on the border between Cameroon and the Central African Republic (figure 4c). It is straightforward to calculate the fraction of the selected area occupied by cassava fields, $A_H A^{-1}$ = 0.011, and, according to figure 4a-b, the corresponding threshold cluster size and separation distances

are $L_H^* = 0.27$km and $\Delta_H^* = 2.29$km. Therefore, were it logistically possible, our analyses indicate that aggregating the crop area from figure 4c into $L_H^* \times L_H^*$ clusters separated by distance Δ_H^* would be characterized by the minimal value of the infection rate $r_{min} = \beta n$.

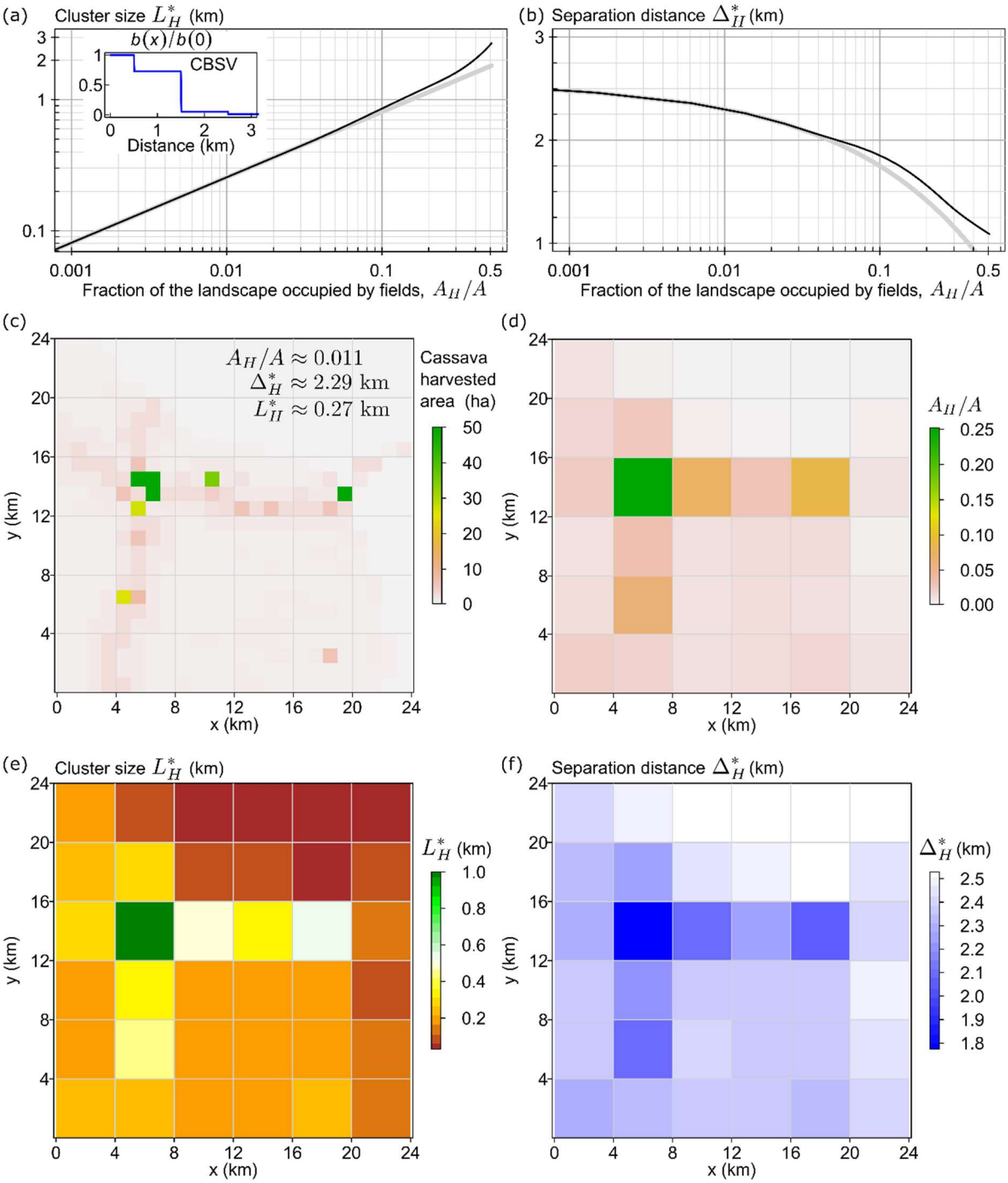

Figure 4. Threshold cluster size L_H^* and threshold separation distance Δ_H^* identified for an example of CBSV dispersal kernel and a cassava landscape. (a)-(b) Threshold cluster size L_H^* and separation distance Δ_H^* that minimise initial infection rate, r, as the fraction of landscape occupied by the host crop increases. Black curves represent numerical estimates obtained from equations (2.6) and (2.7), thick grey curves represent explicit analytical estimates from equations (3.1) and (2.7). **(c)** The

landscape of cassava, given at 1 km spatial resolution. **(d)** The same cassava landscape at 4 km spatial resolution and shown in terms of the fraction of area occupied by the host crop $A_H A^{-1}$. **(e)-(f)** Maps of L_H^* and Δ_H^* calculated by using information from panels (a), (b) and (d), show how maximally aggregated the crop area in each cell could be for the infection rate to remain minimal, i.e. $r_{min} = \beta n$, where the value of n is determined within each cell separately.

However, major redistributions of cropping patterns are unlikely to be practically feasible. Hence, as a more practically relevant situation, we considered smaller 4km-by-4km local areas where local spatial reconfigurations of cropping patterns might potentially be possible. We aggregated the original landscape onto a 4 km spatial resolution (figure 4d). Using values of the fraction of area occupied by the host crop $(A_H A^{-1})$ in each 4 km × 4 km cell, each cell is assigned a corresponding value of L_H^* (figure 4e) and Δ_H^* (figure 4f). These maps show how maximally aggregated the crop area in each cell could be for the infection rate to remain minimal $r_{min} = \beta n$, where the value of n is determined within each cell separately. For an illustration, consider the cell in figure 4d-f located between 4 km and 8 km on the x axis, and between 12 km and 16 km on the y axis. Our analysis shows that the infection rate would remain minimal if cassava fields were aggregated into a cluster of size approximately 1 km × 1 km surrounded by a cassava-free buffer zone with width $\Delta_H^*/2 \approx 900$ m. In the cell located between 16 km and 20 km on the x axis and between 12 km and 16 m on the y axis the infection rate would remain minimal if cassava fields were aggregated into a cluster of size 500 m × 500 m surrounded by a cassava-free buffer zone with width $\Delta_H^*/2 \approx 1$ km.

Maps from figures 4e-f could in principle be used to inform decisions on where to plant new fields of cassava without increasing the risk of early epidemic spread of CBSV. If a $L_H^* \times L_H^*$ cluster of fields already exists within a given 4 km × 4 km cell, then to avoid increasing infection rate the new field should not be placed within the recommended cassava-free buffer zone (with width $\Delta_H^*/2$) around the cluster. New fields could be planted in the vicinity of smaller clusters, but each smaller cluster of size $L_H \leq L_H^*$ should be surrounded by a cassava-free buffer zone with width $\Delta_H/2$ where $\Delta_H = L_H\left(\sqrt{A/A_H} - 1\right)$.

4. Discussion

We have identified approximate analytical expressions (2.6) and (2.7) that determine threshold characteristics for the width (L_H^*) and distance between (Δ_H^*) clusters of susceptible crops that can be used to minimise the risk of invasion at the start of an epidemic. The analysis involves integration of the intrinsic spatial characteristics of pathogen dispersal and distribution of host crops to decelerate invading pathogens over the landscape. Hence, the threshold characteristics, L_H^* and Δ_H^*, are derived in units of the scale parameter, a, of a pathogen dispersal kernel. The analytical approach is effective across a range of scales for a wide class of dispersal kernels and host landscapes. The results are using a Gaussian (figure 2), an exponential power and an inverse power-law (figure 3), and other commonly used dispersal kernels (table B1 and electronic supplementary material, Supplementary Note 4), when tested against simulations involving individual based epidemic models on artificially

generated landscapes. We also carried out a preliminary analysis of a real system using a parameterised landscape-scale spatial epidemic model of the CBSV epidemic (25) and realistically mapped cassava landscape (26). Overall, these results provide valuable epidemiological tool to gain insight in selecting methods required to decelerate the initial spread of an invading pathogen through a landscape of susceptible crops.

We used two main approximations in deriving the analytical results. The first approximation was applied to landscapes where hosts were aggregated into a *small number* of clusters (i.e. where r is a decreasing function of the number of clusters, see e.g. figure 2). In those cases, we estimated r from a single cluster and the corresponding density $\bar{n}_1$ (that is the spatially averaged density of contacts with susceptible crops within a single cluster that can result in infection from an initial randomly infected host), $r \approx \beta\bar{n}_1$, (approximation 1, equation (2.3)). In other landscapes, where crops were aggregated into a *large number* of clusters (i.e. where r depends weakly on the number of clusters, see e.g. figure 2), we used a second approximation and estimated r assuming a constant density, n (that is the density of crops within the entire landscape and therefore independent of the number of clusters), $r \approx \beta n$, (approximation 2). Approximation 1 (where $r \approx \beta\bar{n}_1$) considers only a single cluster and neglects contacts from other clusters, and therefore it underestimates r. In contrast, approximation 2 (where $r \approx \beta n$) may overestimate r by considering contacts with all hosts within the entire landscape. The intersection of the two approximations determines the threshold size L_H^*, i.e. $\beta\bar{n}_1(L_H^*) = \beta n$ (equation 2.5). The underestimation (due to approximation 1) of the left hand side of equation 2.5 and the overestimation on the right hand side (due to approximation 2) lead to an underestimation at the intersection point for the thresholds number of clusters, $N_{clusters}^*$ (figure 1c) and, consequently, to overestimation of L_H^* due to the relationship $L_H^* = \sqrt{A_H/N_{clusters}^*}$. The resulting overestimation of L_H^* provides a practical upper bound to the size of a cluster of crop fields that minimizes the risk of rapid spread during initial stages of epidemics.

By using methods based on r (or R_0 given the link in SIR models as $R_0 = r/\mu$ (18)), our analysis is focused on short-term epidemiological dynamics. The analysis is therefore useful to predict outcomes during initial invasion but it does not necessarily provide an accurate assessment of the long-term dynamics of an epidemic. Nonlinear dynamics, typical of many epidemics, mean that initial fast or slow rates of epidemic progress are not sustained throughout the epidemic. For example, Brown and Bolker (8) and Benicà *et al*. (34) have shown how initially high values of r or R_0 can result in a slow spread of pathogens at later stages of an epidemic in which there are trade-offs between local and long-range dispersal.

Overall, the results of this paper improve our understanding of the relationship between spatial scales of host distribution and pathogen dispersal and their role in epidemic dynamics (4,35). For ease of presentation, we have motivated the method for a pathogen, but it can equally be applied to pest invasions for which dispersal kernels are known or can be estimated. There is potential to use the analytical approach to inform agronomic planning decisions (36) to optimise the size and spacing between clusters of fields in order to minimise

initial infection rate of an invading pathogen Future work could develop the analytical approach further to encompass the role of spatial scales associated with control measure (4,37) on initial epidemic dynamics.

Acknowledgements

The authors are grateful to Dr Stephen Cornell for useful discussions at early stages of this work, and to Dr Alison Scott-Brown for helpful comments on the manuscript. CAG acknowledges financial support from the Bill and Melinda Gates Foundation.

Funding

Y.F.S. and C.A.G. acknowledge support from the Epidemiology and Modelling Group, Cambridge, UK. C.A.G. also acknowledges support from the Bill and Melinda Gates Foundation (INV-010472).

Appendix

Appendix A. Computer simulations of IBM, used in Figure 2

The individual based model (IBM) from Suprunenko *et al.* (18), used in the current paper is a stochastic spatially-explicit IBM that describes invasion and spread of a pathogen through a stationary population of identical square fields of crops located within a square landscape. Each field is characterised by central coordinates and can be in one of two states, susceptible or infected. Fields are aggregated into square clusters that are arranged spatially on a regular square lattice (figure 1a, main text). Within a cluster, fields are arranged on a regular square lattice without overlap or gaps between individual fields. At the start of an epidemic, a single randomly selected field within an entire landscape is infected. The dispersal of a pathogen is described by a product of the dispersal kernel, $b(x)$, and the epidemiological parameter β that denotes the infection rate per contact density (figure 1b, main text). Data (33) in figure 2 correspond to the following parameters used in computer simulations in Suprunenko *et al.* (18): the dispersal kernel $b(x) = \frac{1}{2\pi\sigma^2}\exp\left(-\frac{x^2}{2\sigma^2}\right)$, $\sigma = 10$ km and 1 km; the area of an individual field $A_0 = 0.04$ km^2; the total area of the entire landscapes $A = 365 \times 365$ km^2; the ratio of the area occupied by an agricultural crop, A_H, and the total area, $A_H/A = 0.6, 0.3, 0.15,\ 0.01$; time is measured in units where the rate $\beta = 1$. Using the expected number of infected fields, $I(t)$, calculated as an average over 2000 simulations, the infection rate, r, was estimated as $r = \delta t^{-1} \times \ln[I(\delta t)/I(0)]$ using $\delta t = 0.1$.

Appendix B. Dispersal kernels

We consider dispersal kernels that are widely used in phenomenological approaches in ecology and epidemiology (as summarized by Nathan *et al.* (32)). Dispersal kernels $b(x)$ are normalized in 2D space, $\int_0^\infty \int_0^{2\pi} b(x)x\mathrm{d}x\mathrm{d}\phi = 1$, and include a scale parameter (a) and a shape parameter (b_0), table B1. For each kernel in table B1, the threshold parameters L_H^* and Δ_H^* are determined and shown in this paper, either in figure 3 or in electronic supplementary material, Supplementary Note 4.

Kernel name	Kernel $b(x)$ expression, $a > 0$	Kernel name	Kernel $b(x)$ expression, $a > 0$
(Negative) Exponential	$\frac{1}{2\pi a^2}\exp\left(-\frac{x}{a}\right)$	Gaussian	$\frac{1}{\pi a^2}\exp\left(-\frac{x^2}{a^2}\right)$
(Inverse) Power-law	$\frac{(b_0-2)(b_0-1)}{2\pi a^2}\times,$ $\times\left(1+\frac{x}{a}\right)^{-b_0}, b_0 > 2$	Exponential Power	$\frac{b_0}{2\pi a^2\Gamma\left(\frac{2}{b_0}\right)}\exp\left(-\frac{x^{b_0}}{a^{b_0}}\right),$ $b_0 > 0$
2Dt power-law	$\frac{(b_0-1)}{\pi a^2}\left(1+\frac{x^2}{a^2}\right)^{-b_0},$ $b_0 > 1$	Tophat	$\begin{cases}\frac{1}{\pi a^2}, x \le a \\ 0, x > a\end{cases}$
Logistic	$\frac{b_0\left(1+\frac{x^{b_0}}{a^{b_0}}\right)^{-1}}{2\pi a^2\Gamma\left(\frac{2}{b_0}\right)\Gamma\left(1-\frac{2}{b_0}\right)},$ $b_0 > 2$		

Table B1. Dispersal kernels considered in this paper.

Appendix C. Approximate analytical results for long narrow fields

Here, we consider long narrow fields: we assumed that the landscape with area A contains the number N_{fields} of long narrow fields with size $l \times L_H$ where $l \gg L_H$. The fields are positioned along the y-axis and separated along the x-axis by the distance Δ_H. The area occupied by fields is $A_H = N_{fields} \times l \times L_H$, the total area of the landscape is $A = N_{fields} \times l \times (L_H + \Delta_H)$, and therefore $\Delta_H = L_H \times (AA_H^{-1} - 1)$. The equation that determines the threshold size L_H^*, and an estimate for the threshold width L_H^* of a field when $A_H A^{-1} \ll 1$, i.e. $L_H^* \sim A_H A^{-1} b^{-1/2}(0)$, are derived in electronic supplementary material, Supplementary Note 3.

Appendix D. Effect of increasing spatial scale a on infection rate r

Consider one of the kernels shown in figure 2, and a landscape area with a fixed value of $A_H A^{-1}$. Denote the corresponding value of $L_H^* a^{-1}$ as L_0. Considering two different values of the scale parameter, a_1 and a_2, we have $L_H^{*(1)} = L_0 \times a_1$, and $L_H^{*(2)} = L_0 \times a_2$. Therefore, for $a_1 > a_2$, we have $L_H^{*(1)} > L_H^{*(2)}$. These threshold sizes, $L_H^{*(1)}$ and $L_H^{*(2)}$, correspond to the same value of infection rate, $r_{min} = \beta n$, where $n = A_H A^{-1} A_0^{-1}$. Denote the infection rates corresponding to scale parameters a_1 and a_2 as $r^{(1)}$ and $r^{(2)}$ respectively and consider them on the following two different configurations of the given landscape. First, distributing the given cropped area A_H into clusters of a smaller size, $L_H^{*(2)}$, we would get that both infection rates equal to the minimal rate, $r^{(1)} = r^{(2)} = r_{min}$. Next, re-distributing the cropped area A_H into clusters with larger size $L_H^{*(1)}$ would make no different for infection rate $r^{(1)}$, i.e. $r^{(1)} = r_{min}$, but it would make $r^{(2)}$ larger because $L_H^{*(1)} > L_H^{*(2)}$. Hence, for $a_2 < a_1$ we would get

$r^{(2)} \geq r^{(1)} \geq r_{min}$. In other words, increasing the scale a from a_2 towards a_1 decreases the infection rate of pathogen's dispersal towards its minimal value r_{min}.

References

1. Park AW, Gubbins S, Gilligan CA. Invasion and persistence of plant parasites in a spatially structured host population. Oikos [Internet]. 2001 Jul [cited 2024 Mar 12];94(1):162–74. Available from: https://onlinelibrary.wiley.com/doi/10.1034/j.1600-0706.2001.10489.x

2. Gilligan CA. An Epidemiological Framework for Disease Management. Advances in Botanical Research [Internet]. 2002;38:1–64. Available from: https://doi.org/10.1016/S0065-2296(02)38027-3

3. Stacey AJ, Truscott JE, Asher MJC, Gilligan CA. A Model for the Invasion and Spread of Rhizomania in the United Kingdom: Implications for Disease Control Strategies. Phytopathology [Internet]. 2004 Feb [cited 2024 May 29];94(2):209–15. Available from: https://apsjournals.apsnet.org/doi/10.1094/PHYTO.2004.94.2.209

4. Gilligan CA, Truscott JE, Stacey AJ. Impact of scale on the effectiveness of disease control strategies for epidemics with cryptic infection in a dynamical landscape: an example for a crop disease. J R Soc Interface [Internet]. 2007 Oct 22 [cited 2021 May 3];4(16):925–34. Available from: https://royalsocietypublishing.org/doi/10.1098/rsif.2007.1019

5. Plantegenest M, Le May C, Fabre F. Landscape epidemiology of plant diseases. J R Soc Interface [Internet]. 2007;4(16):963–72. Available from: https://royalsocietypublishing.org/doi/10.1098/rsif.2007.1114

6. Cunniffe NJ, Koskella B, E. Metcalf CJ, Parnell S, Gottwald TR, Gilligan CA. Thirteen challenges in modelling plant diseases. Epidemics [Internet]. 2015 Mar [cited 2024 Jun 26];10:6–10. Available from: https://linkinghub.elsevier.com/retrieve/pii/S1755436514000309

7. Bolker B. Analytic models for the patchy spread of plant disease. Bulletin of Mathematical Biology [Internet]. 1999 Sep [cited 2024 Mar 11];61(5):849–74. Available from: http://link.springer.com/10.1006/bulm.1999.0115

8. Brown D, Bolker BM. The effects of disease dispersal and host clustering on the epidemic threshold in plants. Bulletin of Mathematical Biology [Internet]. 2004 Mar [cited 2024 Mar 11];66(2):341–71. Available from: http://link.springer.com/10.1016/j.bulm.2003.08.006

9. Mikaberidze A, Mundt CC, Bonhoeffer S. Invasiveness of plant pathogens depends on the spatial scale of host distribution. Ecological Applications [Internet]. 2016 Jun [cited 2024 Mar 11];26(4):1238–48. Available from: https://esajournals.onlinelibrary.wiley.com/doi/10.1890/15-0807

10. North AR, Godfray HCJ. The dynamics of disease in a metapopulation: The role of dispersal range. Journal of Theoretical Biology [Internet]. 2017 Apr [cited 2024 Mar 11];418:57–65. Available from: https://linkinghub.elsevier.com/retrieve/pii/S0022519317300371

11. Mundt CC, Sackett KE, Wallace LD. Landscape heterogeneity and disease spread: experimental approaches with a plant pathogen. Ecological Applications [Internet]. 2011 Mar [cited 2024 Mar 11];21(2):321–8. Available from: http://doi.wiley.com/10.1890/10-1004.1

12. Sackett KE, Mundt CC. Effect of plot geometry on epidemic velocity of wheat yellow rust. Plant Pathology [Internet]. 2009 Apr [cited 2024 May 29];58(2):370–7. Available from: https://bsppjournals.onlinelibrary.wiley.com/doi/10.1111/j.1365-3059.2008.01954.x

13. Mundt CC, Leonard KJ. Analysis of factors affecting disease increase and spread in mixtures of immune and susceptible plants in computer-simulated epidemics. Phytopathology [Internet]. 1986;76(8):832–40. Available from: https://www.apsnet.org/publications/phytopathology/backissues/Documents/1986Articles/Phyto76n08_832.PDF

14. Mundt CC. Effect of Host Genotype Unit Area on Development of Focal Epidemics of Bean Rust and Common Maize Rust in Mixtures of Resistant and Susceptible Plants. Phytopathology [Internet]. 1986;76:895–900. Available from: https://www.apsnet.org/publications/phytopathology/backissues/Documents/1986Articles/Phyto76n09_895.PDF

15. Skelsey P, Rossing WAH, Kessel GJT, Van Der Werf W. Invasion of *Phytophthora infestans* at the Landscape Level: How Do Spatial Scale and Weather Modulate the Consequences of Spatial Heterogeneity in Host Resistance? Phytopathology® [Internet]. 2010 Nov [cited 2024 Nov 13];100(11):1146–61. Available from: https://apsjournals.apsnet.org/doi/10.1094/PHYTO-06-09-0148

16. Papaïx J, Touzeau S, Monod H, Lannou C. Can epidemic control be achieved by altering landscape connectivity in agricultural systems? Ecological Modelling [Internet]. 2014;284:35–47. Available from: https://doi.org/10.1016/j.ecolmodel.2014.04.014

17. Rimbaud L, Fabre F, Papaïx J, Moury B, Lannou C, Barrett LG, et al. Models of plant resistance deployment. Annu Rev Phytopathol [Internet]. 2021 Aug 25 [cited 2024 Mar 11];59(1):125–52. Available from: https://www.annualreviews.org/doi/10.1146/annurev-phyto-020620-122134

18. Suprunenko YF, Cornell SJ, Gilligan CA. Predicting the effect of landscape structure on epidemic invasion using an analytical estimate for infection rate. R Soc Open Sci [Internet]. 2024;11:240763. Available from: https://doi.org/10.1098/rsos.240763

19. Suprunenko YF, Gilligan CA. Computer code for: Relationship between spatial scales of pathogen's dispersal and a host landscape that minimizes infection rate in agricultural crops. (In review).

20. Nguyen VA, Bartels DW, Gilligan CA. Modelling the spread and mitigation of an emerging vector-borne pathogen: Citrus greening in the U.S. PLoS Comput Biol [Internet]. 2023 Jun 2 [cited 2024 Mar 11];19(6):e1010156. Available from: https://dx.plos.org/10.1371/journal.pcbi.1010156

21. Cunniffe NJ, Cobb RC, Meentemeyer RK, Rizzo DM, Gilligan CA. Modeling when, where, and how to manage a forest epidemic, motivated by sudden oak death in California. Proc Natl Acad Sci USA [Internet]. 2016 May 17 [cited 2024 Mar 11];113(20):5640–5. Available from: https://pnas.org/doi/full/10.1073/pnas.1602153113

22. Nweke FI, Lynam JK, Spencer DSC. The Cassava Transformation: Africa's Best-Kept Secret [Internet]. Michigan State University Press; 2002. 273 p. Available from: https://www.jstor.org/stable/10.14321/j.ctt7ztc0t

23. Alicai T, Omongo CA, Maruthi MN, Hillocks RJ, Baguma Y, Kawuki R, et al. Re-emergence of cassava brown streak disease in Uganda. Plant Disease [Internet]. 2007 Jan [cited 2024 Mar 12];91(1):24–9. Available from: https://apsjournals.apsnet.org/doi/10.1094/PD-91-0024

24. Muhindo H, Wembonyama F, Yengele O, Songbo M, Tata-Hangy W, Sikirou M, et al. Optimum time for harvesting cassava tubers to reduce losses due to cassava brown streak disease in northeastern DRC. JAS [Internet]. 2020 Apr 15 [cited 2024 Mar 11];12(5):70. Available from: http://www.ccsenet.org/journal/index.php/jas/article/view/0/42480

25. Godding D, Stutt ROJH, Alicai T, Abidrabo P, Okao-Okuja G, Gilligan CA. Developing a predictive model for an emerging epidemic on cassava in sub-Saharan Africa. Sci Rep [Internet]. 2023 Aug 3 [cited 2024 Mar 11];13(1):12603. Available from: https://www.nature.com/articles/s41598-023-38819-x

26. Szyniszewska AM. CassavaMap, a fine-resolution disaggregation of cassava production and harvested area in Africa in 2014. Sci Data [Internet]. 2020 May 27 [cited 2024 Mar 11];7(1):159. Available from: https://www.nature.com/articles/s41597-020-0501-z

27. van den Bosch F, Helps J, Cunniffe NJ. The basic-reproduction number of infectious diseases in spatially structured host populations. Oikos [Internet]. 2024 Jun 18 [cited 2024 Jul 7];e10616. Available from: https://nsojournals.onlinelibrary.wiley.com/doi/10.1111/oik.10616

28. Wadkin LE, Holden J, Ettelaie R, Holmes MJ, Smith J, Golightly A, et al. Estimating the reproduction number, R 0 , from individual-based models of tree disease spread. Ecological Modelling [Internet]. 2024 Mar [cited 2024 Mar 11];489:110630. Available from: https://linkinghub.elsevier.com/retrieve/pii/S030438002400019X

29. Suprunenko YF, Cornell SJ, Gilligan CA. Analytical approximation for invasion and endemic thresholds, and the optimal control of epidemics in spatially explicit individual-based models. J R Soc Interface [Internet]. 2021 Mar [cited 2024 Mar 11];18(176):rsif.2020.0966, 20200966. Available from: https://royalsocietypublishing.org/doi/10.1098/rsif.2020.0966

30. Ovaskainen O, Finkelshtein D, Kutoviy O, Cornell S, Bolker B, Kondratiev Y. A general mathematical framework for the analysis of spatiotemporal point processes. Theor Ecol [Internet]. 2014 Feb [cited 2024 Mar 11];7(1):101–13. Available from: http://link.springer.com/10.1007/s12080-013-0202-8

31. Cornell SJ, Suprunenko YF, Finkelshtein D, Somervuo P, Ovaskainen O. A unified framework for analysis of individual-based models in ecology and beyond. Nat Commun [Internet]. 2019 Oct 17 [cited 2024 Mar 11];10(1):4716. Available from: https://www.nature.com/articles/s41467-019-12172-y

32. Nathan R, Klein E, Robledo-Arnuncio JJ, Revilla E. Dispersal kernels: review. In: Dispersal ecology and evolution. OXFORD UNIV PRESS; 2012. p. 187–210.

33. Suprunenko YF, Cornell SJ, Gilligan CA. Data from: Predicting the effect of landscape structure on epidemic invasion using an analytical estimate for infection rate [Internet]. Figshare; 2024. Available from: https://doi.org/10.6084/m9.figshare.25804702

34. Benincà E, Hagenaars T, Boender GJ, Van De Kassteele J, Van Boven M. Trade-off between local transmission and long-range dispersal drives infectious disease outbreak size in spatially structured populations. Ferrari M (Matt), editor. PLoS Comput Biol [Internet]. 2020 Jul 6 [cited

2024 May 29];16(7):e1008009. Available from: https://dx.plos.org/10.1371/journal.pcbi.1008009

35. Gilligan CA. Sustainable agriculture and plant diseases: an epidemiological perspective. Phil Trans R Soc B [Internet]. 2008 Feb 27 [cited 2024 Nov 13];363(1492):741–59. Available from: https://royalsocietypublishing.org/doi/10.1098/rstb.2007.2181

36. Vega D, Ibarra S, Varela Pardo RA, Poggio SL. Agroecological management of crop diseases: a review. Agroecology and Sustainable Food Systems [Internet]. 2023 Aug 9 [cited 2024 Nov 13];47(7):919–49. Available from: https://www.tandfonline.com/doi/full/10.1080/21683565.2023.2216149

37. Meentemeyer RK, Haas SE, Václavík T. Landscape Epidemiology of Emerging Infectious Diseases in Natural and Human-Altered Ecosystems. Annu Rev Phytopathol [Internet]. 2012 Sep 8 [cited 2024 May 29];50(1):379–402. Available from: https://www.annualreviews.org/doi/10.1146/annurev-phyto-081211-172938